Physica D 405 (2020) 132354

Contents lists available at ScienceDirect

Physica D

journal homepage: www.elsevier.com/locate/physd

Extracting a mixing parameter from 2D radiographic imaging of variable-density turbulent flow

S. Kurien [a,*], F.W. Doss [b], D. Livescu [c], K. Flippo [d]

[a] Theoretical Division, T-3, Los Alamos National Laboratory, Los Alamos, NM 87545, United States of America
[b] Theoretical Design Division, XTD-IDA, Los Alamos National Laboratory, Los Alamos, NM 87545, United States of America
[c] Computer and Computational Sciences Division, CCS-2, Los Alamos National Laboratory, Los Alamos, NM 87545, United States of America
[d] Physics Division, P-24, Los Alamos National Laboratory, Los Alamos, NM 87545, United States of America

ARTICLE INFO

Article history:
Available online 11 February 2020
Communicated by V.M. Perez-Garcia

Keywords:
Turbulence models
Variable-density turbulence
Radiographic imaging

ABSTRACT

We extract a suitably averaged fluctuating density from the two-dimensional radiographic image of a flow. The X-ray attenuation is given by the Beer–Lambert law which exponentially damps the incident beam intensity by a factor proportional to the density, opacity and thickness of the target. By making reasonable assumptions for the mean density, opacity and effective thickness of the target flow, we estimate the density fluctuation contribution to the attenuation. The extracted density fluctuations averaged across the thickness of the flow in the direction of the beam may be used to form the density–specific-volume correlation b. In a statistical description of variable-density turbulence, b quantifies the degree of mixedness. The ability to extract a measure of mixedness from experimental data would be a powerful tool that could be used in the validation of mix models. The scheme proposed is tested for DNS data computed for variable density buoyancy-driven mixing. We quantify the deficits in the extracted value of b due to target thickness, Atwood number and modeled signal noise. This analysis justifies using the proposed scheme to infer the mix parameter from thin targets at moderate to low Atwood numbers. To illustrate how the scheme might be used in a practical problem, we demonstrate its application to a radiographic image of counter-shear flow obtained from experiments at the National Ignition Facility.

Published by Elsevier B.V.

1. Introduction

Experimental platforms such as the National Ignition Facility (NIF) at the Lawrence Livermore National Laboratory [1,2] and the OMEGA laser at the Laboratory for Laser Energetics [3] are designed to facilitate measurements of fluid dynamics events that result from laser pulses impinging on suitably designed targets. Among the diagnostic tools used to study these events are radiographic images taken from various angles relative to the target. The resulting images, which may be taken at any prescribed time after the laser is shot, are a 2-dimensional (2D) representation of flow structure. A visualization of such an image might show the positions of, for example, instabilities and their spatial extent, and perhaps retain some information on the relative positions of various components of the target. However, quantitative information on density variances and mixing, in particular, are not directly available. If such information were to be deduced from the radiographic images, it would be very useful in parameterizing physical processes in model calculations of such flows. This process is standard in improving predictive capabilities of models for complex flow systems.

Approaches to modeling turbulent mixing have often been motivated by the causative instabilities such as Rayleigh–Taylor and Richtmyer–Meshkov instabilities. Youngs was an early proponent of the need to model such instabilities, developing a two-fluid modeling approach as well as extensive early numerical simulations and analysis of RT instability driven turbulence [4,5]. Since those efforts, RT and RM instability validation have remained a mainstay of turbulence model development. The NIF and OMEGA platforms offer a unique platform for imaging such instability driven hydrodynamic flows. However, such images of flow structures evolved from instabilities do not give a quantitative measure of the mixing itself. If such measures could be recovered from radiographic data, they would provide powerful new ways to constrain and validate models.

In this paper we propose a way to extract a statistical measure of mixing from 2D radiographic images. The data obtained in this way is essentially photon counts through the target. The attenuation of an X-ray beam through a target depends on the thickness, density and opacity of the target via the Beer–Lambert law. We do not, in principle, know all of the three parameters

* Corresponding author.
E-mail address: skurien@lanl.gov (S. Kurien).

https://doi.org/10.1016/j.physd.2020.132354
0167-2789/Published by Elsevier B.V.

a priori. However, using reasonable assumptions for any two of the parameters, we can invert the attenuation law to recover information about the third. In our particular case we show how to recover a statistical measure of the density fluctuations which will then be used to compute a mixing parameter.

We approach the problem of computing a mixing parameter at the level of equations for single-point, second-order correlations in variable-density turbulence. One such modeling framework is the BHR model [6] which was developed at Los Alamos National Laboratory to address the problem of mix modeling in multi-physics codes. While we will use the BHR model and its description of mixing in what follows, it is worth emphasizing at the outset that the algorithm developed below for extraction of a mixing parameter from radiographic data permits straightforward application to analogous quantities in other modeling frameworks that lie within the Reynolds- or Favre-averaged family of single-point closure models for turbulence. The *k-L* [7] and Reynolds stress [8] models are two examples of alternative RANS models for which a mixing parameter, suitably defined, may be analyzed in a manner similar to what follows. In particular, the proposed algorithm does not depend on how well the model performs in a particular flow or what the underlying modeling assumptions are. Once a mix parameter that is defined based solely on density fluctuations is identified, our approach can be used to approximate it from radiographic data.

Variable-density turbulence consists of the mixing and transport of two fluids of different densities that are permitted to interpenetrate and mix driven by an acceleration (e.g. gravity or laser impulse). The second-order equations of motion are discussed at length in [6] wherein a closure model is formulated at the level of the second-order single-point correlations. We review this approach here briefly in order to introduce the quantity of interest for this study. We begin with the choice of Favre decomposition for the velocity field:

$$u_i = \tilde{u}_i + u_i'' \tag{1}$$

where the mass-weighted (Favre averaged) velocity $\tilde{u}_i = \frac{\overline{\rho u_i}}{\overline{\rho}}$ and u_i'' is the fluctuation with respect to the Favre averaged mean velocity. The equations for the fluctuations defined in this way are obtained from the Navier–Stokes equations. Subsequently, the equation for single-point correlations of the fluctuations $R_{ij} = \overline{\rho u_i'' u_j''}$ gives rise to a pressure-gradient production term $a_n \frac{\partial \overline{p}}{\partial x_n}$ where $a_i = -\overline{u_i''}$ may now be interpreted as the velocity corresponding to mass flux. This requires a further equation for a_i which gives rise to a second pressure-gradient production term $b\frac{\partial \overline{p}}{\partial x_i}$ where $b = -\overline{\rho' v'}$ for the specific-volume fluctuations defined by $v' = v - \overline{v}$ where $v = 1/\rho$, The density–specific-volume correlation b, also called the density self-correlation may be re-written as $b = \frac{\overline{(\rho')^2}}{\rho\overline{\rho}}$ which implies that b is non-negative. The detailed closed form of BHR includes additional equations for a length-scale, energy-dissipation and conservation of species which we will not present or discuss here.

The quantity of interest to us in the present work is

$$b = -\langle \rho' v' \rangle \tag{2}$$

where ρ' is the density fluctuation and v' is the specific volume fluctuations; $\langle\cdot\rangle$ denotes a suitable average over the domain or over an ensemble. As described in the introduction, the factor b modulates the pressure gradient which generates the mass flux, which in turn governs the conversion from potential to kinetic energy. Production of kinetic energy stirs the flow. b may be shown to be positive, only going to zero when the flow is molecularly mixed. Given these properties, b might be considered to be a good measure of the mixing state of the flow.

The variable density case provides a non-trivial test bed for non-Boussinesq effects in the mix problem. The parameter b can be written to separate out the Boussinesq contribution using a Taylor series expansion for small density fluctuations [9]:

$$b = \frac{\langle \rho'^2 \rangle}{\rho_0^2} - \frac{\langle \rho'^3 \rangle}{\rho_0^3} + \cdots \tag{3}$$

$$= \sum_{n\geq 2}^{\infty} (-1)^n \frac{\langle \rho'^n \rangle}{\rho_0^n} \tag{4}$$

$$= \sum_{n\geq 2}^{\infty} (-1)^2 \frac{\langle \rho'^{*n} \rangle}{A^n} \tag{5}$$

where $\rho_0 = \langle \rho \rangle$ is the mean density over the domain. The last equality expresses the expansion in terms of the non-dimensional Atwood number parameter A and ρ'^* is normalized by one half the different between the pure fluid densities. The series truncated at the first term $n = 2$ is the Boussinesq component. In the paper we will assess the importance of the non-Boussinesq contributions both from studying the terms in this expansion as well as direct measurements from DNS of different Atwood numbers.

The paper is divided into five sections. Section 2 describes how to derive a statistical measure of density that would result in an observed attenuation, and calculate an estimate of b. In Section 3 we apply the method to data obtained from DNS of variable density gravity-driven flow for which we know all statistical quantities exactly. We use the DNS data as the target for a test incident beam and compute estimates for b and compare them to the exact quantities to assess the accuracy of our inversion procedure. We quantify the deficits inherent in the attenuation process due to the target thickness, Atwood number and non-Boussinesq effects and noise in the incident beam. In Section 4 we apply the procedure to infer statistical estimates of a mix parameter from a sample image obtained from NIF experiment designed to study the development of shear instability in a thin Titanium tracer foil that is counter-sheared by shocks generated by simultaneous laser impulse at both ends of the foil. A summary and discussion are presented in Section 5.

2. Inversion algorithm

Let $\hat{\boldsymbol{z}}$ denote the direction of incident beam of intensity I_0 in a conventional right-handed Cartesian coordinate system denoted by unit-vectors $(\hat{\boldsymbol{i}}, \hat{\boldsymbol{j}}, \hat{\boldsymbol{k}})$. Then the Beer–Lambert law for the beam intensity upon exiting the target is given by

$$I(x, y) = I_0 \exp\Big(-\int_0^{Z_0} \rho(\boldsymbol{x})\kappa(\boldsymbol{x})\mathrm{d}z\Big) \tag{6}$$

x and y are the cartesian position coordinates in the plane orthogonal to z; ρ and κ are respectively the spatially varying density and opacity of the material at vector position $\boldsymbol{x} = (x\hat{\boldsymbol{i}}, y\hat{\boldsymbol{j}}, z\hat{\boldsymbol{k}})$; Z_0 is the linear distance through which the beam travels. Indeed the experimental data available are essentially the function $\Gamma(x, y) = \ln\Big(\frac{I_0}{I(x,y)}\Big)$. From this function we attempt to extract quantitative information about the density fluctuations and a mixing parameter as follows.

Define the average of a quantity f in the n direction by

$$\langle f \rangle_n = \frac{1}{N}\int_0^N f \mathrm{d}n \tag{7}$$

where n may be x, y or z and N is the upper bound of the n coordinate in the flow. Then, attenuation through the flow as a

function of position (x, y) in the plane may be written as:

$$\Gamma(x,y) = \ln\Big(\frac{I_0}{I(x,y)}\Big) = \kappa_0 Z_0 \langle \rho(x,y,z)\rangle_z = \kappa_0 Z_0 \rho(x,y) = \kappa_0 Z_0 (\rho_0 + \rho'(x,y)) \tag{8}$$

where the planar average $\rho(x, y)$ is expressed in terms of the global mean ρ_0 and fluctuations about the mean $\rho'(x, y)$ at a given (x, y). We could just as well have used the more refined definition of $\rho_0 = \langle\rho\rangle_{z,y}$ but this does not add anything relative to our test case which is 3D homogeneous; this choice is also motivated by the fact that we will not have *a priori* knowledge of structures and inhomogeneities in the actual experimental and therefore (near) statistical homogeneity is a reasonable first assumption. The reader will note that in Eq. (8) the opacity κ_0 and the thickness Z_0 are modeled as constants. It is not easy to confirm this from data of the type we are ultimately interested in analyzing, but should be a reasonable assumption for a large enough class of situations. A suitable fluctuating density can stand as a surrogate for the effects of both opacity and thickness variation if we consider an effective mass attenuation constant $\mu = \kappa\rho$. The first term of Eq. (8) corresponds to an optical depth (or inverse Knudsen number), being a ratio of the characteristic flow size Z_0 to a radiation mean free path $L_R = 1/(\rho_0\kappa_0)$, while the second term might be interpreted as a fluctuating Knudsen number.

From Eq. (8) we may infer the density fluctuations in the plane in terms of the experimentally known quantities and material properties:

$$\rho'(x,y) = \frac{\Gamma(x,y)}{\kappa_0 Z_0} - \rho_0. \tag{9}$$

and similarly the specific-volume fluctuations in the plane:

$$\upsilon'(x,y) = \frac{1}{\rho(x,y)} - \Big(\frac{1}{\rho(x,y)}\Big)_0 = \frac{\kappa_0 Z_0}{\Gamma(x,y)} - \Big(\frac{\kappa_0 Z_0}{\Gamma(x,y)}\Big)_0 \tag{10}$$

where again the subscript 0 denotes a mean-value over the domain. The fluctuation quantities defined by Eqs. (9) and (10) describe an infinitesimally thin layer with material distributed such that the net effect of the X-ray beam attenuation through that layer is the same as the effect of the attenuation through the original three-dimensional domain. We define the experimentally inferred surrogate for b,

$$b_{Se} = \langle \rho'(x,y)\upsilon'(x,y)\rangle \tag{11}$$

where ρ' and υ' are given by Eqs. (9) and (10) respectively. What is lost in this description, is any detailed information of the fluctuations in the direction of attenuation. Therefore, in a radiographic imaging experiment, beam attenuation represents an *a priori* averaging of density fluctuations in one (beam) direction. Any subsequent inference of density fluctuation *statistics* or *correlations* necessarily uses such averaged quantities with some inherent loss of detail about the flow.

To emphasize this point, let us suppose that one does have the detailed information about density at all points in the domain.Then the mix parameter may be computed for any averaging scheme as follows. In the plane orthogonal to the beam direction the functional form of b is,

$$b(x,y) = \langle \rho'(\boldsymbol{x})\upsilon'(\boldsymbol{x})\rangle_z \tag{12}$$

where the point-wise fluctuations $\rho'(\boldsymbol{x}) = \rho(\boldsymbol{x}) - \rho_0$ and ρ_0 is the mean density over the entire domain. An analogous definition holds for $\upsilon'(\boldsymbol{x})$. and along, say, the x-direction, by further averaging

$$b(x) = \langle b(x,y)\rangle_y = \langle \rho'(\boldsymbol{x})\upsilon'(\boldsymbol{x})\rangle_{z,y} \tag{13}$$

and finally down to a single-point quantity defined over the entire domain

$$b = \langle b(x)\rangle_x = \langle \rho'(\boldsymbol{x})\upsilon'(\boldsymbol{x})\rangle_{z,y,x} \tag{14}$$

If, however, one can only infer a statistical value of the density fluctuations in the plane as in Eqs. (9) and (10), then a type of surrogate value of b might be estimated as:

$$b_S(x) = \langle \rho'(x,y)\upsilon'(x,y)\rangle_y \tag{15}$$

where,

$$\rho'(x,y) = \langle \rho(\boldsymbol{x})\rangle_z - \rho_0 \tag{16}$$

$$\upsilon'(x,y) = \langle 1/\rho(\boldsymbol{x})\rangle_z - \upsilon_0 \tag{17}$$

may be calculated exactly from DNS data. The inferred density fluctuation in Eq. (9) is consistent with the above definition in Eq. (16). However, the specific-volume inferred from experiments in Eq. (10) is inconsistent with the definition of Eq. (17). This is because the average in the z-direction of the point-wise specific-volume $\langle 1/\rho(\boldsymbol{x})\rangle_z$ only approaches the inverse of the z-averaged density $1/\langle\rho(\boldsymbol{x})\rangle_z$ in the Boussinesq limit wherein density fluctuations are small. For an experimental measurement using radiography, the choice υ' from Eq. (10) is the only one and we will denote the corresponding mix parameter as b_{Se}. We propose that b_{Se} computed using quantities from radiographic data in this way, is a reasonable approximation for b_S and hence the true b. We will evaluate this hypothesis using calculations of the different measures of υ' from DNS data as a surrogate for the experimental system. In the next section we will use DNS data to compute the mixing parameter both exactly and in its surrogate forms from the radiographic field generated by an assumed initial X-ray beam. The goal is to understand the deficits implicit in an experimentally computed b.

3. Test case: DNS of homogeneous variable density flow

We use as our test case Direct Numerical Simulations (DNS) data of homogeneous buoyancy driven variable density turbulence [10]. This flow is described by the variable-density Navier–Stokes equations, which represent the incompressible (infinite speed of sound) limit of the compressible Navier–Stokes equations with two miscible species with different molar masses [9–11]. In this limit, the density variations arise from compositional changes as the two species mix and lead to non-zero divergence of velocity. The boundary conditions are triply periodic, and the two fluids are initialized as random blobs, consistent with the homogeneity assumption. The flow starts from rest, with only a small amount of dilatational velocity necessary to satisfy the divergence condition and turbulence is generated as the two fluids start moving in opposite directions due to differential buoyancy forces. These forces are generated due to a constant gravity term ρg_z, acting in the vertical direction z in the momentum equations [10]. However, as the fluids become molecularly mixed, the buoyancy forces decrease and at some point the turbulence starts decaying. The flow has similarities with the inner region of the mixing layer generated by the acceleration-driven Rayleigh–Taylor instability during the growth stage and the shock-driven Richtmyer–Meshkov instability during the decay stage [12–14]. As a canonical flow to study variable density effects on turbulence, this flow has also been used to calibrate turbulence models, including the model targeted by our analysis [15].

The test problem is set up as follows. An incident beam of X-rays with intensity $I_0 = 1$ is assumed to enter the box of fluid at $z = 0$ and exit at $z = 1$. We assume that the attenuation is dominated by density fluctuations and set constant $\kappa_0 = 1.0$. The density at each point in the flow domain has been computed as

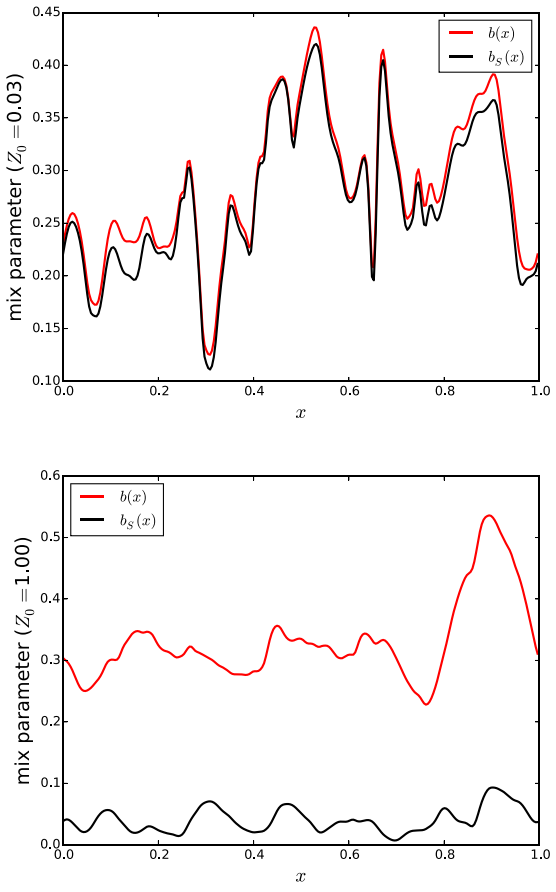

Fig. 1. Comparison of exact $b(x)$ (red) with the surrogate value $b_S(x)$ (black) for averages over a thin slice (top) and full thickness (bottom) of the flow domain.

the DNS solution [9,10]. We considered a snapshot of the flow at the time the turbulent kinetic energy reaches its peak, so that the flow has a rich turbulent structure. At this time the Atwood number is 0.75 and the mean density $\rho_0 = 4.0$ in the units of the simulation. As explained in [9] turbulence in homogeneous variable-density turbulence at the time of peak kinetic energy is similar to various canonical turbulence problems, including the inner region of the fully developed Rayleigh–Taylor mixing layer.

3.1. Effect of target thickness

We first assess whether the surrogate $b_S(x)$ defined in Eq. (15) is indeed a good approximation of the true $b(x)$ defined in Eq. (13). In Fig. 1 we show these quantities computed both over a thin slice of the domain with thickness $Z_0 = 0.03$ and then over the full domain with thickness $Z_0 = 1.0$. As may be expected, for the thin domain, the actual and surrogate values agree quite well, while the disparity is significant for averages over the full domain.

We computed the error as a function of the non-dimensional thickness Z_0/L_ρ where L_ρ is the integral length scale of the density variable tabulated for the decaying flow as a function of A in Table 1. The standard error is defined as

$$\sigma_b = \sqrt{\frac{\sum_x (b_S(x) - b(x))^2}{N_x}} \tag{18}$$

where $N_x = 256$ is the number of data points in the x-direction. The error is shown in Fig. 2 for different A as the flow decays. As the thickness becomes smaller than L_ρ the error scales as Z_0^2 while the growth is a shallower $Z_0^{1/2}$ as the thickness increases past L_ρ.

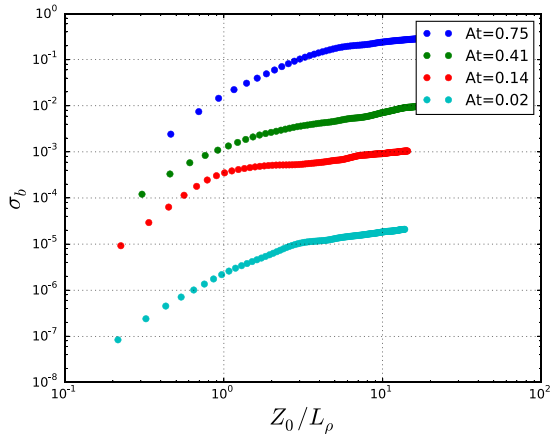

Fig. 2. Standard error relative of $b_S(x)$ relative to $b(x)$ as a function of domain thickness.

Table 1
Integral length scale L_ρ of the density variance as a function of the Atwood number as the flow evolves.

A	L_ρ
0.75	0.034
0.41	0.051
0.14	0.069
0.02	0.072

This result demonstrates that for attenuation through sufficiently thin slices of a statistically homogeneous flow, the surrogate definition of the mix parameter is justified. This is reassuring in terms of application of these methods to real data for which the actual density fluctuations are not known. The NIF experiments that provide the motivation for the present analysis appear to fall in the regime of 'thin' domains for which the inversion algorithm we propose might be justified.

We proceed in the next section to assess the effect of non-Boussinesq effects on the surrogate measurement of b_S.

3.2. Effect of Atwood number

Given the above justification for using b_S as a reasonable surrogate for the true b for thin domains, we now proceed to assess the difference arising in b_S with definitions for υ' given by Eqs. (10) and (17).

From the attenuation formula Eq. (6) we obtain the radiographic image of the data as shown in Fig. 3. The attenuation ranges from almost total (blue regions) to about 85% (red regions). From this intensity field we can infer $\rho'(x, y)$ using both Eqs. (9), as inferred from the test attenuation field, and (16). These are identical and the resulting field is shown in Fig. 4. However a comparison of υ' computed from the attenuated field according to Eq. (10) and from Eq. (17) shows a difference (see Fig. 5). As discussed above, this discrepancy is due to non-Boussinesq effects, pointing to an Atwood number (A) dependence. The global Atwood number in this DNS flow decays over time as the flow mixing. We can therefore track the discrepancy introduced by the Boussinesq effects by tracking b_S computed in two ways over time.

We compare the exact $b_S(x)$ as defined in Eq. (15) and its estimate $b_{Se}(x)$ using the quantities defined in Eqs. (9) and (10) at two different times in the flow corresponding to two different global Atwood numbers 0.75 and 0.14. Fig. 6 shows these results.

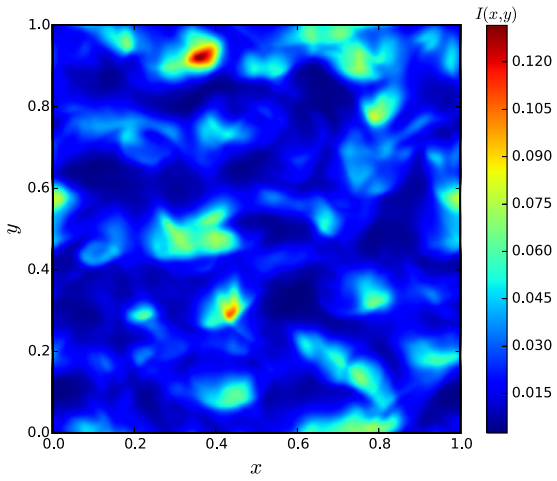

Fig. 3. Map of intensity field $I(x, y)$ after attenuation in the z-direction through variable density flow data.

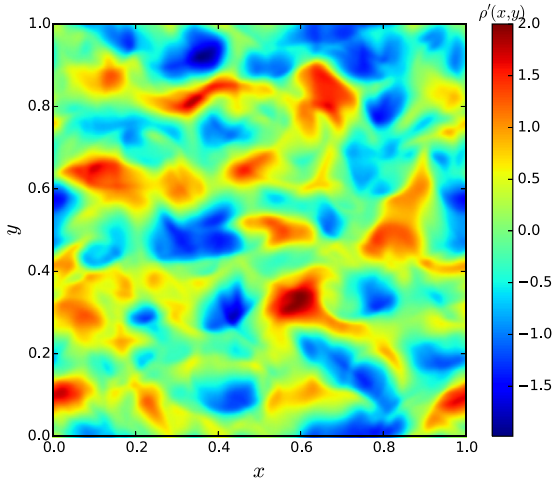

Fig. 4. Two-dimensional field of density fluctuations $\rho'(x, y)$. The calculation from Eq. (9) shown here (inferred from $I(x, y)$ in Fig. 3) agrees with the direct calculation from the DNS data using Eq. (16) (not shown).

The Atwood number dependence may be further quantified by considering the error

$$\sigma_{b_S} = \sqrt{\frac{\sum_x (b_S(x) - b_{Se}(x))^2}{N_x}}. \tag{19}$$

This quantity is plotted for Atwood number as the flow decays at four different times; the result is shown in Fig. 7. The error is calculated for attenuation through the whole domain $Z_0 = 1.0$ and for attenuation through thickness equal to the integral scale of the density $Z_0 = L_\rho$. The relative error decays rapidly with A for both cases, justifying the use of the estimated b_{S_e} at moderate to low A. These errors are relatively small compared to the error implicit in thickness effects. The two errors become comparable for thin target domains, that is, for $Z_0 \leq L_\rho$ (see Fig. 2).

3.2.1. Taylor-series expansion of b and non-Boussinesq effects

We recall that the parameter b may be expanded in a Taylor series for small υ' as described in the Introduction (Eq. (5)) with the leading order capturing the Boussinesq contribution. We compute the series expansion b_E for n up to 6. In the expansion, ρ' is inferred from Γ, (Eq. (9)) and ρ_0 is the mean over the domain. Fig. 8 shows that the series b_E converges to $b_{Se}(x)$ over most of the domain indicating consistency with the definitions. However, also consistent with expectation, the deficit between b_{Se} and b_S is not recoverable. That is lost in the averaging implicit in the attenuation process itself.

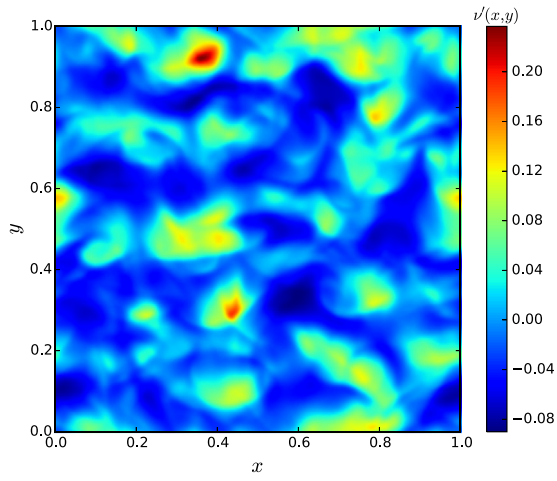

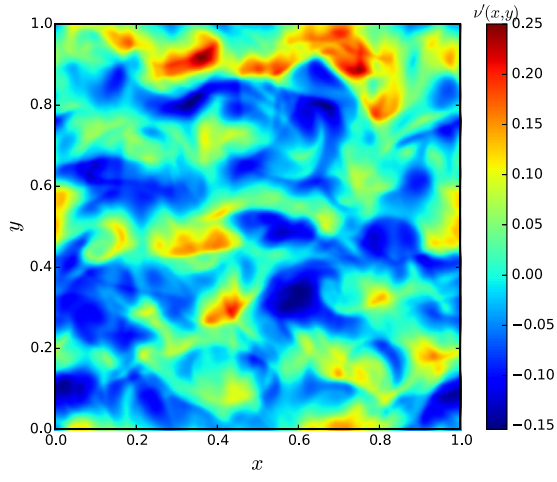

Fig. 5. Two-dimensional specific-volume $\upsilon'(x, y)$ inferred from the X-ray image as in Eq. (10) (top); and computed according to Eq. (17) (bottom).

The analysis thus far shows that the optimal procedure is to estimate b_{Se} from the attenuated intensity field. This will be close to b_S at low to moderate A. Then, assuming a thin target (relative to some dynamically significant scale such as the density integral length scale), b_S becomes a true surrogate of b.

In the next section we consider the effect of noise on the attenuation and the resulting inferred statistics.

3.3. Effect of noise

Experimental data will typically be noisier than DNS data. In this section we make a reasonable ansatz for the noise in the incident beam and compute the resulting variability in the inferred density statistics. Since the incident beam is a positive definite signal, we choose a Gamma-distribution for I_0 with shape k and scale θ. The mean of a gamma distribution is $k\theta$. We therefore choose values of k and θ such that $k\theta = 1$. That is, we model a system with mean incident X-ray intensity of 1.0 and vary the shape of the distribution around this mean. Fig. 9 shows the effect of adding noise in the incident beam for two different values of θ at $A = 0.75$ for attenuation through the entire box. The estimated $b_{S\theta}(x)$ (defined by b_{Se} with input noise) in fact

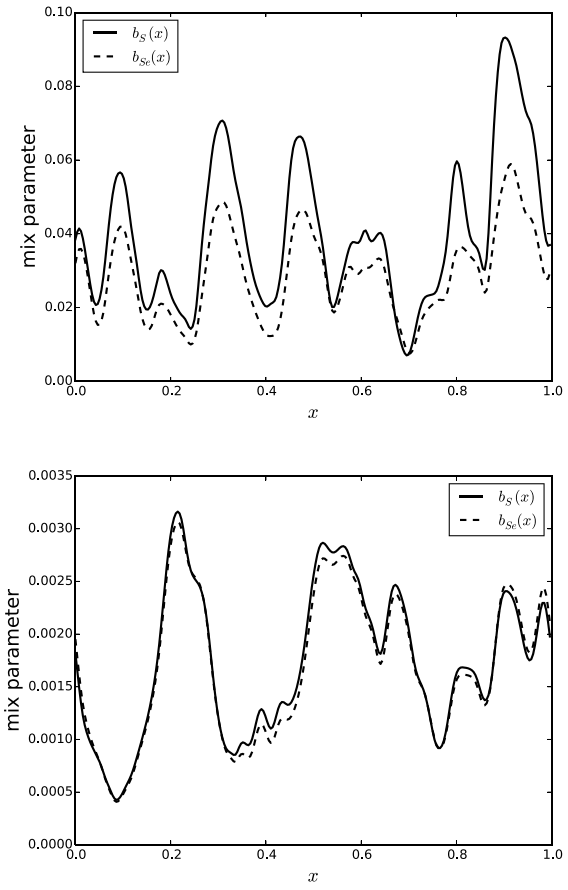

Fig. 6. Exact $b_S(x)$ computed from Eq. (15) compared with its estimate from the radiography data at $A = 0.75$ (top) and $A = 0.14$ (bottom).

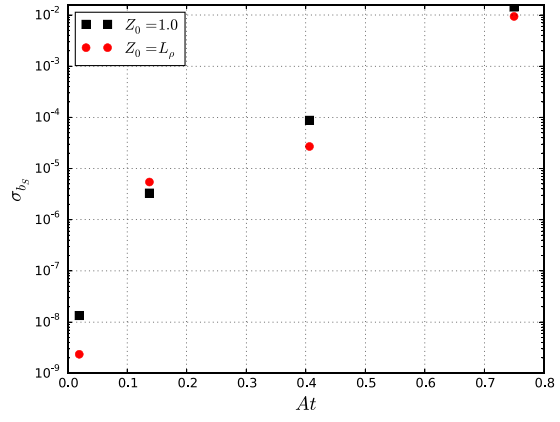

Fig. 7. Atwood number dependence of the standard error σ_{b_S} of $b_{Se}(x)$ relative to b_S.

shows better agreement with the target $b_S(x)$ for small values of θ. The noise appears to artificially decrease the error relative to b_S for small θ. This observation is strengthened in Fig. 10. Denoting the estimated mix parameter as $b_{S\theta}$, we compute the error

$$\sigma_{b\theta} = \sqrt{\frac{\sum_x (b_S(x) - b_{S\theta}(x))^2}{N_x}}. \tag{20}$$

For each A the error goes to a different lower bound for sufficiently small θ. It is interesting to note that for each A there is a lower bound on the error. As θ approaches 1, the relative error

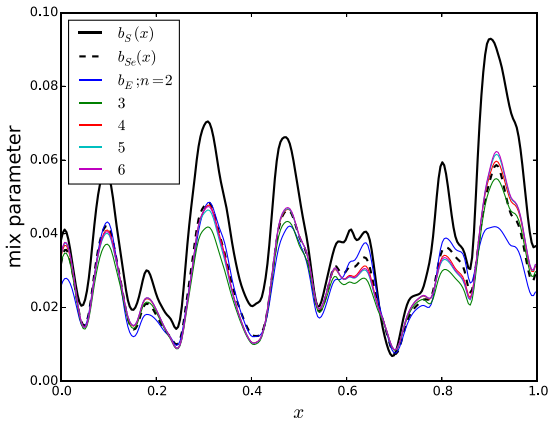

Fig. 8. The surrogate function b_S, its estimate b_{Se} from the radiography inversion, and the series expansion b_E at $A = 0.75$. The series b_E converges (magenta line, $n = 6$) to b_{Se} (dashed line).

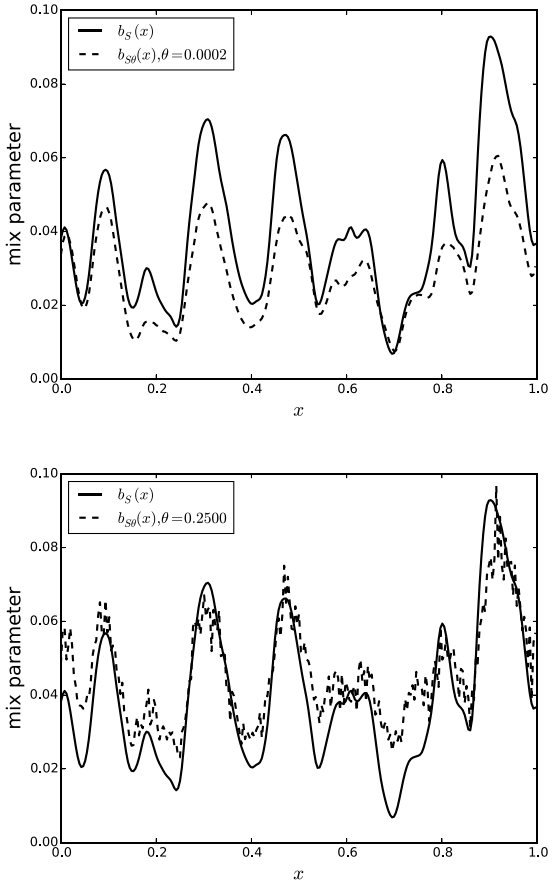

Fig. 9. The surrogate mix parameter $b_S(x)$ compared with a noisy inferred value $b_{S\theta}$ for two values of the noise parameter θ from a gamma-distribution of initial intensity I_0. Top: $\theta = 0.0002$; bottom: $\theta = 0.25$.

becomes independent of A. There also appears to be an Atwood-independent regime for the error introduced by noise in a band of values $0.1 \leq \theta \leq 1$. We conclude from this simple noisy model analysis that a small amount of noise could in fact 'help' by artificially pushing the inferred $b_{S\theta}$ closer to b_S. However, since there is still some deficit due to the fact that $b_{S\theta}$ is a modification of b_{Se} (which is the best we can obtain from experiment), we never reduce the error relative to b_S to zero at any A. That is, the

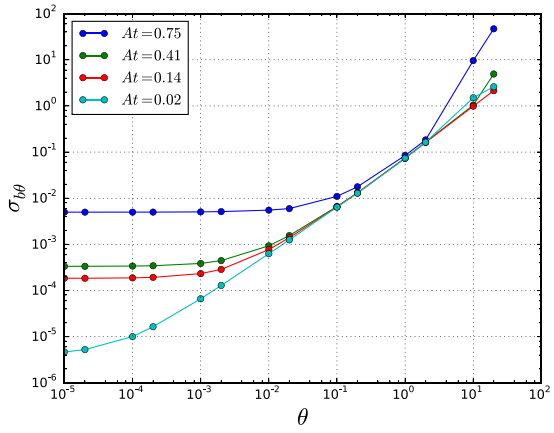

Fig. 10. Dependence on noise distribution parameter θ of the standard error relative to $b_S(x)$ for various Atwood numbers.

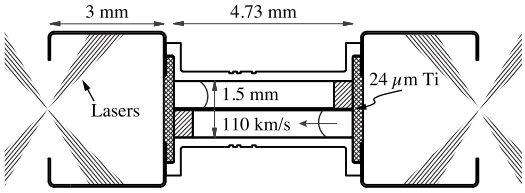

Fig. 11. Schematic of counter-shear experiment.

Table 2
List of exact (top row) and approximate measurements of the mixing parameter. Each row has the definition and whether it can be measured in DNS or radiographic experiments.

$b(x)$	$\langle \rho'(\boldsymbol{x})v'(\boldsymbol{x})\rangle_{z,y}$	DNS
$b_S(x)$	$\langle \rho'(x,y)v'(x,y)\rangle_y$ using Eqs. (16) and (17)	DNS
$b_{Se}(x)$	$\langle \rho'(x,y)v'(x,y)\rangle_y$ using Eqs. (9) and (10)	DNS, expt
$b_E(x)$	$\sum_{n\geq 2}^{\infty}(-1)^n \frac{\langle \rho'^n\rangle}{\rho_0^n}$	DNS
$b_{S\theta}(x)$	b_{Se} for noisy I_0	DNS

noise model does not compensate entirely (even if artificially) for the loss of information about density fluctuations.

Table 2 lists the various definitions of b used in this study. In summary thus far, the analysis of DNS data has shown that the target thickness is a key factor in whether a reasonable mix parameter b_S may be extracted from radiographic data. For domains of thickness less than the integral length scale of the density field, the approximation $b_S(x) \simeq b(x)$ seems to be justified. The Atwood number dependence is independent of target thickness, and errors associated with A are smaller than those of thickness effects. Finally, for small values of the scale parameter θ, the error relative to $b_S(x)$ is artificially decreased.

4. Extraction of mix parameter from the radiographic image of a counter-sheared flow

In this section we perform a calculation to demonstrate the utility of our scheme in a practical application. The main purpose is to step through the process of deriving a mixing parameter from radiographic data supplemented with knowledge of relevant experimental conditions and material properties. Since we do not have density measurements yet to confirm our results, as can be done with DNS, we use our validation and assessment of the method for DNS data above, along with the associated caveats, to justify application to experimental data.

Fig. 11 shows the experiment geometry — a 5 mm long beryllium shock tube with inner diameter 1.5 mm is driven by the

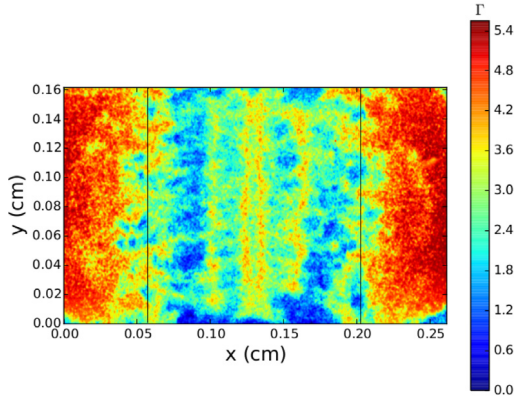

Fig. 12. Plane-view of the function Γ for the counter-shear flow in a *Ti* target generated by opposing shocks moving in the x-direction, at $t = 34.5$ ns after initiation of the experiment. The vertical black lines enclose the mixing region of interest.

National Ignition Facility [1] on both sides by 330 kJ, shining into gold hohlraums mounted on either end. This fills the hohlraums with a 250 eV radiation bath, which ablates a plastic reaction mass (shown in crosshatch in the schematic) and drives a strong shock into each side of the tube. The tube interior is filled with two hemicylinders of light foam, bisected by a metal foil: here, 24 μm of solid density titanium. Gold hemi-cylindrical plugs are placed on opposite sides of each end of the tube to collimate the shocks, so that they break separately into opposite sides of the shock tube. The laser drive is sustained for 11 ns, allowing an approximately steady flow of around 110 km/s to set up behind each shock. When the shocks cross in the tube center, this creates a region of intense shear across the foil. Furthermore, the drive heats the tube environment to over 50 electron volts (around 600,000 K), driving it into the dense plasma regime, allowing it to respond hydrodynamically to the drive. The experiment survives until approximately 36 ns, at which point the shock tube disintegrates under the high pressure and temperature and the experiment ends.

The experiment is diagnosed by reserving 100 kJ of the available laser energy drive to later irradiate a iron foil placed outside of the shock tube. The heated foil then emits X-rays which pass through the shock tube and are imaged by an opposing camera system, with time resolution around 0.1 ns. Experiment materials are chosen such that the diagnostic X-rays pass preferentially through the tube and low density foam, but are absorbed by the titanium. The facility geometry only allows this data to be taken in one direction per experiment; the experiment is then repeated to image the mixing layer in an orthogonal direction. Sample images are shown in the x-z plane (the edge view, Fig. 13) and in the orthogonal plane imaging down through the planar titanium layer (Fig. 12). More information on the facility configuration and experiment including details on the laser drive and auxiliary diagnostics can be found in [16–19] and on the X-ray diagnostic scheme in [20,21].

We choose a representative frame from a series of shots completed at NIF for counter-shear flow in Titanium (Ti) target of initial thickness of 24 μm [22]. Both planar and edge views of the target are available at identical time $t = 34.5$ ns. The planar view (orthogonal to beam in the z-direction) of the function Γ is shown in Fig. 12 while the edge view is in Fig. 13. In the planar view, the equivalent of $\Gamma(x, y)$ is directly imaged while in the edge view the intensity is in photon counts. The edge-view in this type of experiment has been used extensively to infer a mix-width based on the thickness over which the intensity is damped to, say, 90% of maximum [18].

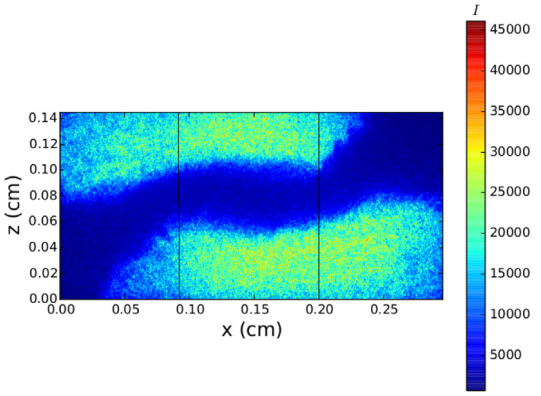

Fig. 13. Edge-view of the X-ray intensity field for counter-shear flow in a *Ti* target generated by opposing shocks moving in the x-direction, at $t = 34.5$ ns after initiation of the experiment. The vertical black lines enclose the mixing region of interest.

Table 3
Experimental data parameters for *Ti* target at shot time $t = 34.5$ μs.

Target	ρ_i (g/cc)	Z_i (cm)	κ_0 (cm^2/g)	Z_0 (cm)	ρ_0 (g/cc)
Ti	4.5	0.0024	203.7	0.06	0.208

From these data parameters we need to obtain the quantities κ_0, Z_0 and ρ_0 in order to solve for the effective fluctuations in the plane as defined in Eqs. (9) and (10). We will use the mix-width for this dataset as the thickness $Z_0 = 0.06$ cm reported in [23]. The value of the opacity is estimated from the cold flat-field data (prior to start of experiment) using the initial relation

$$\Gamma_i = \kappa_0 \rho_i Z_i \tag{21}$$

where the subscript i denotes initial ($t = 0$) values. The initial flat-field image had a uniform attenuation of 11% through the target, that is, $I/I_0 = 0.11$ giving $\Gamma_i = \ln(I/I_0) = 2.2$. The initial density of the target *Ti* is $\rho_i = 4.5$ g/cc. Eq. (21) may be solved giving $\kappa_0 = 203.7$ cm^2/g. In practice, when the density fluctuations are multiplied by the specific-volume in Eq. (11), the actual value of κ_0 drops out, so we are only sensitive to our choices for this value if we want to check intermediate calculations.

To estimate the mean density ρ_0 at shot-time, we use the internal consistency of the data, requiring that:

$$\rho_0 = \left\langle \frac{\Gamma(x,y)}{\kappa_0 Z_0} \right\rangle_{x,y} \tag{22}$$

Restricting the average to the region that is thought to be the mix region (excluding the peripheral regions which have ablator and other contaminants) this yields $\rho_0 = 0.20$ g/cc. As a check we can use the fact that the thickness increases by a factor of $Z_0/Z_i = 25$ to scale the density so that $\rho_0 = \rho_i/25 = 0.18$ g/cc. There is good agreement between the two estimates given that the mix region at this stage is defined somewhat arbitrarily. Indeed one might be justified in narrowing the Γ field for the mix region even further, or even prescribe a more sophisticated non-constant mix-width consistent with the visual impression of the radiograph (Fig. 12) so that the ρ_0 estimated is arbitrarily close to 0.18 g/cc which we may think of as a lower bound. We will use the latter value in the remaining analysis. Similarly, the magnitude of Z_0 drops out of the final calculation of b, but may be useful for checking intermediate calculated values. The main given and inferred parameters of the experimental data are summarized in Table 3.

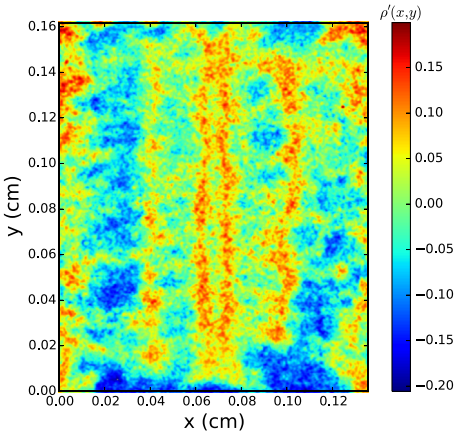

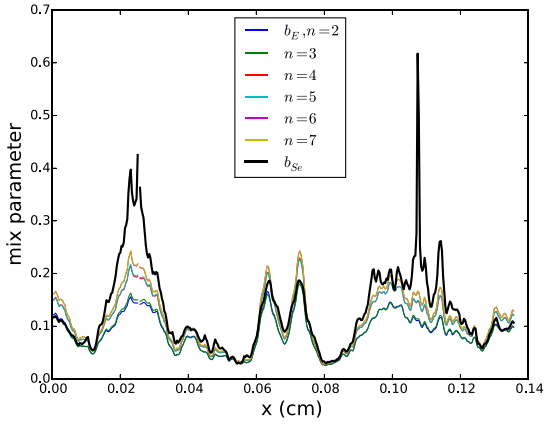

Fig. 14. Mix parameter for NIF *Ti* data.

The procedure to extract $b_{Se}(x)$ is followed as for the DNS test case example above. We also compute the expansion $b_E(x)$ and show it for up to $n = 7$ in Fig. 14. The figures show that the mixing parameter retains the structure of the flow quite well, that is, the positions of the "roll-ups" are captured. The solid thick black line represents b_{Se}; the series expansions appear to converge to b_{Se} from below for lower values of b; with exception of the very high valued regions where the series tends to converge but falls significantly short of the experimentally extracted value of b_{Se}. The notable exception to this behavior is observed for the two central features at 0.065 and 0.075 cm, corresponding to the central pair of roll-up structures. Here the Boussinesq approximation at $n = 2$ (blue line) approximates b_{Se} (thick black line) quite well while approximations with higher-order contributions ($n > 3$) overshoot and converge to values larger than b_{Se}. It must be recalled that in the case of the experiments we do not have information on the true value of the density fluctuations, since what we extract is a surrogate, or effective, density fluctuation field. Assuming that the target thickness is small enough, we may speculate that the deficits between the expansion and the value of b_{Se} may be due to invalidity of the expansion itself in strongly non-Boussinesq regimes (for example, near the coherent vortical structures, where baroclinic torques become important [24]). The negligible contribution of odd-n terms reflects the near-symmetry of the problem in the x-direction.

5. Conclusion

Our goal in this study was to develop a method to extract quantitative information about turbulent mixing processes from

radiographic images of hydrodynamic flows. The quantity of interest is the density–specific-volume correlation function $b = -\langle \rho' v' \rangle$. This mixing parameter arises in a second-order statistical representation of the equations for variable density turbulence, and its value goes to zero as the flow becomes molecularly mixed. Two-dimensional radiographic images essentially offer photon counts which, when the incident beam details are known, may be associated with an averaged density fluctuation profile by inverting the Beer–Lambert attenuation law. From such a density fluctuation profile, approximate functional forms for b may be derived. The main approximation arises from the attenuation process itself, which is an intrinsic loss of information due to averaging that is proportional to the finite thickness of the target. The dependence on proximity to Boussinesq approximation may be used to quantify Atwood number (A) dependence.

Our derived approximations for b are evaluated using high-resolution data from Direct Numerical Simulations (DNS) of variable density buoyancy-driven turbulence. Since the simulations offer the exact b, we can assess the quality of the approximations imposed due to target thickness and Atwood number. The target thickness is the dominant effect in most cases, and clearly so for the lowest $A = 0.02$. Anticipating noisy data from experiments, we also performed test of how the results may be affected if a noisy incident beam is used. The effect of moderate noise is also subdominant to target thickness effects.

With the understanding that thin targets at moderate to low Atwood number are suitable candidates from which to extract hydrodynamic mixing parameters, we next applied the new algorithm to experimentally acquired radiographic data from the NIF facility. This was done not attempting to exhaustively identify all possible sources of experimental uncertainties, but to demonstrate that the method tested against DNS data may be applied to suitably reduced laboratory flows in a straightforward manner. The width of the structures in these data appears to be of the same order as the thickness of the mixing layer, thus placing us in the 'thin' target regime, thus justifying this type of exercise. The results from application of the inversion algorithm to extract an approximate b profile showed good agreement with the locations and intensities of the 'roll-ups' and other gross features of the flow. A series approximation with leading order Boussinesq terms shows poor agreement with the data in the highly unmixed regions; this is not surprising since the flow is likely in parameter regimes outside the weakly non-Boussinesq regime for which the series approximation is valid. The latter observation reaffirms the importance of estimating b directly, using the procedure outlined in this paper.

There have been different formulations of statistical measures of mixing proposed in other models. For example [8] evolves the square of the density fluctuations while [25,26] are examples of modeling approaches that evolve the square of the specific-volume fluctuations. Both of these may be interpreted as descriptive of mixing. Since both these rely on knowledge of density fluctuations, our method would allow for either of these alternative formulations to be extracted in a manner formally analogous to what has been described above. However, only the combination of density and specific-volume in b will be insensitive to inferred mixing layer properties κ_0 and Z_0, and may require correspondingly greater care to estimate.

In future work, more quantitative assessments for b computed from the experiments will be done in conjunction with simulations that compute b dynamically for the flows of interest.

Acknowledgments

We are pleased to be able to present these results to this special issue of Physica D in honor of the numerous and long-standing contributions of Prof. David Youngs in the field of turbulence modeling and instabilities. We thank R. Lowrie for useful comments on the draft. Computational resources for the DNS simulations were provided by the LANL Institutional Computing (IC) Program. This work has been authored by employees of Triad National Security, LLC which operates Los Alamos National Laboratory under Contract No. 89233218CNA000001 with the U.S. Department of Energy/National Nuclear Security Administration. The authors acknowledge funding from the LANL/NNSA Office of Experimental Sciences, United States program; SK was also partially funded by LANL, United States Advanced Simulation and Computing under the Physics and Engineering Models, Mix and Burn project.

References

[1] E.I. Moses, C.R. Wuest, The National Ignition Facility: Status and plans for laser fusion and high-energy-density experimental studies, Fusion Sci. Technol. 43 (3) (2003) 420–427.

[2] S.R. Nagel, K.S. Raman, C.M. Huntington, S.A. MacLaren, P. Wang, M.A. Barrios, T. Baumann, J.D. Bender, L.R. Benedetti, D.M. Doane, S. Felker, P. Fitzsimmons, K.A. Flippo, J.P. Holder, D.N. Kaczala, T.S. Perry, R.M. Seugling, L. Savage, Y. Zhou, A platform for studying the Rayleigh–Taylor and Richtmyer–Meshkov instabilities in a planar geometry at high energy density at the National Ignition Facility, Phys. Plasmas 24 (7) (2017) 072704, http://dx.doi.org/10.1063/1.4985312, arXiv:https://doi.org/10.1063/1.4985312.

[3] F.W. Doss, E.N. Loomis, L. Welser-Sherrill, J.R. Fincke, K.A. Flippo, P.A. Keiter, Instability, mixing, and transition to turbulence in a laser-driven counterflowing shear experiment, Phys. Plasmas 20 (2013) 012707.

[4] D.L. Youngs, Numerical simulation of turbulent mixing by Rayleigh–Taylor instability, Physica D 12 (1) (1984) 32–44, http://dx.doi.org/10.1016/0167-2789(84)90512-8, URL http://www.sciencedirect.com/science/article/pii/0167278984905128.

[5] D.L. Youngs, Modelling turbulent mixing by Rayleigh–Taylor instability, Physica D 37 (1) (1989) 270–287, http://dx.doi.org/10.1016/0167-2789(89)90135-8, URL http://www.sciencedirect.com/science/article/pii/0167278989901358.

[6] D.C. Besnard, F.H. Harlow, R.M. Rauenzahn, Los Alamos National Laboratory Report No. LA-10911-MS.

[7] G. Dimonte, R. Tipton, K-l turbulence model for the self-similar growth of the Rayleigh–Taylor and Richtmyer-Meshkov instabilities, Phys. Fluids 18 (8) (2006) 085101, http://dx.doi.org/10.1063/1.2219768, arXiv:https://doi.org/10.1063/1.2219768.

[8] O. Grégoire, D. Souffland, S. Gauthier, A second-order turbulence model for gaseous mixtures induced by Richtmyer—Meshkov instability, J. Turbul. 6 (2005) N29, http://dx.doi.org/10.1080/14685240500307413, arXiv:https://doi.org/10.1080/14685240500307413.

[9] D. Livescu, J.R. Ristorcelli, Variable-density mixing in buoyancy-driven turbulence, J. Fluid Mech. 605 (2008) 145–180.

[10] D. Livescu, J.R. Ristorcelli, Buoyancy-driven variable-density turbulence, J. Fluid Mech. 591 (2007) 43–71.

[11] D. Livescu, Numerical simulations of two-fluid turbulent mixing at large density ratios and applications to the Rayleigh–Taylor instability, Phil. Trans. R. Soc. A 371 (2013) 20120185.

[12] D. Livescu, J.R. Ristorcelli, R.A. Gore, S.H. Dean, W.H. Cabot, A.W. Cook, High–Reynolds number Rayleigh–Taylor turbulence, J. Turbul. 10 (13) (2009) 1–32.

[13] Y. Zhou, Rayleigh–Taylor and Richtmyer–Meshkov instability induced flow, turbulence, and mixing. I, Phys. Rep. 720 (2017) 1–136.

[14] Y. Zhou, Rayleigh–Taylor and Richtmyer–Meshkov instability induced flow, turbulence, and mixing. II, Phys. Rep. 723 (2017) 1–160.

[15] J.D. Schwarzkopf, D. Livescu, J.R. Baltzer, R.A. Gore, J.R. Ristorcelli, A two length-scale turbulence model for single-phase multi-fluid mixing, Flow Turbul. Combust. 96 (2016) 1–43.

[16] F.W. Doss, J.L. Kline, K.A. Flippo, T.S. Perry, B.G. DeVolder, I. Tregillis, E.N. Loomis, E.C. Merritt, T.J. Murphy, L. Welser-Sherrill, J.R. Fincke, The shock/shear platform for planar radiation-hydrodynamics experiments on the national ignition facility, Phys. Plasmas 22 (2015) 056303.

[17] F.W. Doss, K.A. Flippo, E.C. Merritt, Observation and analysis of emergent coherent structures in a high-energy-density shock-driven planar mixing layer experiment, Phys. Rev. E 94 (2016) 023101.

[18] F.W. Doss, K.A. Flippo, D. Capeli, T. Cardenas, B. DeVolder, J. Kline, L. Kot, S. Kurien, E. Loomis, E.C. Merrit, T. Perry, D. Schmidt, C.D. Stefano, Increasing shot and data collection rates of the shock/shear experiment at the national ignition facility, J. Phys. Conf. Ser. 717 (2016) 012059.
[19] K.A. Flippo, F.W. Doss, J.L. Kline, E.C. Merritt, D. Capelli, T. Cardenas, B. DeVolder, F. Fierro, C.M. Huntington, L. Kot, E.N. Loomis, S.A. MacLaren, T.J. Murphy, S.R. Nagel, T.S. Perry, R.B. Randolph, G. Rivera, D.W. Schmidt, Late-time mixing sensitivity to initial broadband surface roughness in high-energy-density shear layers, Phys. Rev. Lett. 117 (2016) 225001.
[20] K.A. Flippo, J.L. Kline, F.W. Doss, E.N. Loomis, M. Emerich, B. Devolder, T.J. Murphy, K.B. Fournier, D.H. Kalantar, E. Merritt, T.S. Perry, I. Tregillis, L. Welser-Sherrill, J.R. Fincke, Development of a big area BackLighter (BABL) for high energy density experiments, Rev. Sci. Instrum. 85 (2014) 093501.
[21] K.A. Flippo, B. DeVolder, F. Doss, J. Kline, E. Loomis, D. Capelli, D. Schmidt, M.K. Schmitt, The laser-driven X-ray big area backlighter (BABL): Design, optimization, and evolution, J. Phys. Conf. Ser. 717 (2016) 012062.
[22] K.A. Flippo, F.W. Doss, B. Devolder, J.R. Fincke, E.N. Loomis, J.L. Kline, L. Welser-Sherrill, Investigating turbulent mix in HEDLP experiments, J. Phys.: Conf. Ser. 688 (2016) 012018.
[23] F.W. Doss, J.L. Kline, K.A. Flippo, T.S. Perry, B.G. DeVolder, I. Tregillis, E.N. Loomis, E.C. Merritt, T.J. Murphy, L. Welser-Sherrill, J.R. Fincke, The shock/shear platform for planar radiation-hydrodynamics experiments on the National Ignition Facility, Phys. Plasmas 22 (2015) 056303.
[24] Joly, Reinaud, Chassaing, The baroclinic secondary instability of the two-dimensional shear layer, Phys. Fluids 12 (2000) 2489.
[25] D. Souffland, O. Soulard, J. Griffond, Modeling of Reynolds-stress models for diffusion fluxes inside shock waves, J. Fluids Eng. 136 (9) (2014) 091102–091102–4, http://dx.doi.org/10.1115/1.4027381.
[26] J. Griffond, O. Soulard, Evaluation of augmented rsm for interaction of homogeneous turbulent mixture with shock and rarefaction waves, J. Turbul. 15 (9) (2014) 569–595, http://dx.doi.org/10.1080/14685248.2014.919395, arXiv:https://doi.org/10.1080/14685248.2014.919395.